

## Squeezing Bose-Bose liquid drops

A. Sanuy <sup>1</sup>, R. Barač <sup>2</sup>, P. Stipanović <sup>2</sup>, L. Vranješ Markić <sup>2,\*</sup> and J. Boronat <sup>1</sup>

<sup>1</sup>*Departament de Física, Universitat Politècnica de Catalunya, Campus Nord B4-B5, E-08034 Barcelona, Spain*

<sup>2</sup>*Faculty of Science, University of Split, Ruđera Boškovića 33, HR-21000 Split, Croatia*



(Received 26 October 2023; accepted 21 December 2023; published 16 January 2024)

We explore ultradilute Bose-Bose liquid droplets squeezed by an external harmonic potential in one spatial direction. Our theoretical study is based on a functional that is built using quantum Monte Carlo results of the bulk phase and incorporates finite-range effects. A characteristic feature of these drops is the existence of a critical atom number, which is the minimum number of particles to have a many-body bound state. We report results on the critical atom numbers for different magnetic fields and applying confinement strengths towards a quasi-two-dimensional setup. In the regime where the local-density approximation is expected to be valid, we find that the critical atom number decreases linearly with the harmonic oscillator length of the confining potential. With the largest squeezing explored in our work, we predict stable drops containing from approximately 1000 to 2000 atoms for magnetic fields from 56.230 to 56.574 G, respectively. Our functional reduces the critical numbers for any confinement and applied magnetic field with respect to the estimations based on the Lee-Huang-Yang model. We observe saturated drops when the number of atoms in the drop is much larger than the critical value, their central density being higher for the quantum Monte Carlo functional than for the Lee-Huang-Yang one.

DOI: [10.1103/PhysRevA.109.013313](https://doi.org/10.1103/PhysRevA.109.013313)

### I. INTRODUCTION

Ultradilute liquid droplets were predicted by Petrov [1] and soon after confirmed in experiments with a Bose-Bose mixture of two hyperfine states of  $^{39}\text{K}$  [2,3]. These many-body bound states arise from the interplay between attractive interspecies and repulsive intraspecies interactions, and, in this sense, they differ from the unicomponent classical or quantum helium droplets that result from the interplay between the repulsive short-range and attractive long-range components of the interatomic potential. The delicate balance between attractive and repulsive interactions produces Bose-Bose drops which are extremely dilute, with densities that are orders of magnitude smaller than the ones of liquid helium. In fact, very dilute self-bound systems with dipolar atoms were experimentally noticed even before, arising from the interplay of short-range repulsion and attractive head-to tail dipolar moments [4–6]. Further experimental efforts have resulted in heterogeneous Bose-Bose droplets [7,8] of  $^{41}\text{K}$ - $^{87}\text{Rb}$  and  $^{23}\text{Na}$ - $^{87}\text{Rb}$ . The emergence of these new ultradilute liquids has been recently reviewed in Refs. [9,10].

According to mean-field theory, binary mixtures of Bose-Einstein condensates become unstable against collapse when the attractive interspecies interaction overcomes the repulsive contact potential between atoms [11]. However, in the ultradilute liquid phase the mean-field collapse is avoided if beyond-mean-field first-order perturbative corrections, in the form of the Lee-Huang-Yang (LHY) energy functional [12,13], are included. This correction, which takes into

account quantum fluctuations, is repulsive and thus it can stabilize attractive Bose-Bose mixtures [1]. Going beyond the LHY corrections, the formation of Bose-Bose droplets was also observed using the first-principles diffusion Monte Carlo (DMC) method [14].

In the Bose-Bose mixture, the LHY functional suffers from an intrinsic inconsistency, with the appearance of an imaginary term in the energy for densities different from the equilibrium one. It has been suggested that this drawback can be eliminated by introducing bosonic pairing [15,16] or time-dependent Hartree-Fock-Bogoliubov theory [17]. This is at variance with a single-component Bose gas, where no such imaginary term appears and where the LHY term is able to explain accurately the departure of the energy from the mean-field prediction [18,19]. Furthermore, observed properties [2] of an ultradilute mixture of two hyperfine states of  $^{39}\text{K}$  showed deviations from the predictions of the theory based on interactions described solely in terms of  $s$ -wave scattering lengths [1], suggesting the inclusion of finite-range corrections beyond LHY. The dependence of the energy on the effective range was noticed in a variational hypernetted-chain Euler-Lagrange calculation [20] and confirmed later on by the study of ultradilute liquids with the DMC method [21]. Interestingly, those DMC simulations showed that, by including the effective range, the universality of the theory can be extended [21,22]. The improved energy functionals with built-in knowledge of both  $s$ -wave scattering lengths and the effective ranges allowed approaching experimental results for the critical atom number [22], as well as addressing excitation spectra [23,24] and the study of the previously observed [25] dynamics of equilibration and collisions of  $^{39}\text{K}$  droplets [26].

\*Corresponding author: leandra@pmfst.hr

The interest in ultradilute droplets was very soon extended to low-dimensional systems, where it was found that in two dimensions (2D) the liquid phase is formed whenever the intraspecies interactions are repulsive and the interspecies one is attractive [27]. LHY correction was also studied in the crossover from three to two dimensions and from three to one dimensions [28,29], which provided conditions for the use of three-dimensional (3D) local-density functionals to study droplets in confinement. Recently, Bose-Bose droplets squeezed by an external harmonic potential in one spatial direction have been studied using the modified gapless Hartree-Fock-Bogoliubov method [30], without assuming the local-density approximation in the direction of squeezing [31].

Previous research shows that departures from mean-field + LHY predictions (MFLHY) are stronger when the mixtures are compressed [22]. It would be particularly interesting, for the range of the experimentally accessible magnetic fields, to investigate how the critical atom numbers change as the droplet is squeezed, as well as how the density profiles of drops change. The properties of more strongly compressed Bose-Bose mixtures, where quantum fluctuations will be even more prominent, have not been studied using density functional theory incorporating information on the effective range. In the present work, we extend our previous study of confined drops [22] to regimes of stronger confinements, reaching the boundary of the expected validity of the local-density approximation [28].

The paper is organized as follows. In Sec. II, we briefly introduce the density functional approach used in our study, as well as the MFLHY functional. The results on the droplet energies, critical atom numbers, and droplet profiles, for different magnetic fields and squeezing strengths, are presented in Sec. III. Finally, Sec. IV is devoted to summary and conclusions.

## II. METHODS

We study Bose-Bose mixtures of two hyperfine states of  $^{39}\text{K}$  at zero temperature, using the density functional approach. The many-body wave function is built as a product of single-particle orbitals  $\psi_{1,2}$ ,

$$\Psi(\mathbf{r}_1, \mathbf{r}_2, \dots, \mathbf{r}_N) = \prod_{i=1}^{N_1} \psi_1(\mathbf{r}_i) \prod_{j=N_1+1}^{N_2} \psi_2(\mathbf{r}_j), \quad (1)$$

where  $N_1$  ( $N_2$ ) are the number of particles of the first (second) component. The single-particle wave functions are obtained solving the Schrödinger-like equation of motion for each species,

$$i\hbar \frac{\partial \psi_i}{\partial t} = \left( -\frac{\hbar^2}{2m} \nabla^2 + V_{\text{ext}}(\mathbf{r}) + \frac{\partial \mathcal{E}_{\text{int}}}{\partial \rho_i} \right) \psi_i, \quad (2)$$

where  $m$  is the  $^{39}\text{K}$  atomic mass, and  $\mathcal{E}_{\text{int}}$  is an energy per volume term that accounts for the interparticle correlations. The density of each component is  $\rho_i = |\psi_i|^2$ . For the external potential, we have chosen a harmonic confinement in the  $z$  direction,  $V_{\text{ext}} = m\omega_z^2 z^2/2$ , with  $\omega_z = \hbar/(ma_{\text{ho}}^2)$ . There is no confining potential in the  $x$  and  $y$  directions. In the reference

experiment [2], the same confinement potential was applied with oscillator length  $a_{\text{ho}} = 0.639 \mu\text{m}$ . As we are interested in the effect of squeezing on the properties of the drops, we have taken further compression,  $a_{\text{ho}} = f \times 0.639 \mu\text{m}$ , with  $f = 0.9, 0.75, 0.5$ , and  $0.25$ .

In the following, we consider  $^{39}\text{K}$  mixtures at the optimal relative atom concentration yielded by mean-field theory, namely,  $N_1/N_2 = \sqrt{a_{22}/a_{11}}$  [1]. It is worth noticing that this optimal ratio between numbers of particles of both types has been confirmed in DMC simulations [22]. Keeping this ratio fixed, the coupled differential equations (2) can be reduced to a single one, which is a function of the total density  $\rho$ .

For these mixtures, it was shown that the energy per atom, using the data obtained from the DMC calculations, can be accurately written as [22]

$$\frac{E}{N} = \alpha\rho + \beta\rho^\gamma. \quad (3)$$

The parameters  $\alpha$ ,  $\beta$ , and  $\gamma$  were determined in Ref. [22] by fits to the DMC results obtained for the model potential which satisfied both the  $s$ -wave scattering lengths and the effective ranges. The values of these parameters for the range of experimentally relevant magnetic fields, from  $B = 56.23$  G to  $B = 56.639$  G, are given in the Appendix, together with relevant scattering lengths. This allows us to obtain the part of the functional describing interparticle correlations through the relation  $\mathcal{E}_{\text{int}} = \rho E/N$ .

For a couple of reference cases, we performed calculations using the MFLHY functional. Working at the optimal concentration, the energy per particle can be written as in Eq. (3),

$$\frac{E/N}{|E_0|/N} = -3\left(\frac{\rho}{\rho_0}\right) + 2\left(\frac{\rho}{\rho_0}\right)^{3/2}, \quad (4)$$

with  $E_0/N$  being the energy per atom at equilibrium,

$$E_0/N = -\frac{25\pi^2\hbar^2|a_{12} + \sqrt{a_{11}a_{22}}|^3}{768ma_{22}a_{11}(\sqrt{a_{11}} + \sqrt{a_{22}})^6}, \quad (5)$$

and  $\rho_0$  being the equilibrium density,

$$\rho_0 = \frac{25\pi}{1024a_{11}^3} \frac{(a_{12}/a_{11} + \sqrt{a_{22}/a_{11}})^2}{(a_{22}/a_{11})^{3/2}(1 + \sqrt{a_{22}/a_{11}})^4}. \quad (6)$$

In Eqs. (5) and (6),  $a_{ij}$  are the three different  $s$ -wave scattering lengths, whose values for the selected magnetic fields are given in Ref. [22].

We are interested in finding the minimum energy configuration. Therefore, we solve the differential equation (2) in imaginary time  $\tau \equiv it$ . The details are given in the Appendix.

## III. RESULTS

As commented in the Introduction, one of the characteristics of Bose-Bose drops is the requirement of the number of particles being larger than a certain critical atom number,  $N_c$ . This number is very sensitive to the applied magnetic field and to the transversal confinement and, moreover, to the theory applied to obtain it. We calculate the energy of the drops and estimate the minimum atom number that keeps the drop self-bound, which is the number that gives zero binding energy. This study is carried out for each confinement strength,

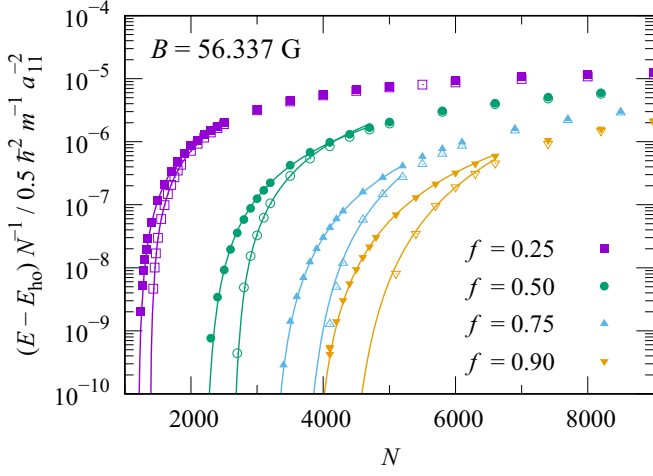


FIG. 1. Total energy of the droplet per particle as a function of the number of particles for the magnetic field  $B = 56.337$  G and several confinements, described by harmonic oscillator lengths  $a_{ho} = f \times 0.639 \mu\text{m}$ . The energies are obtained using both the QMC (solid symbols) and MFLHY (empty symbols) energy functionals. The lines are fits using Eq. (7).

described by the harmonic oscillator length  $a_{ho} = f \times 0.639 \mu\text{m}$ . After subtracting the single-particle energy contribution due to the harmonic oscillator potential, the energies per particle of drops, as a function of the atom number, are fitted to the functional form

$$\epsilon(N) = 10^{-\alpha/(N-N_c)^\beta}, \quad (7)$$

from which the critical atom number  $N_c$  is determined. The dependence of the energies on the cluster size and the fitting model (7) are presented in Fig. 1 for the magnetic field strength  $B = 56.337$  G, using the two density functionals, QMC and MFLHY. For both approaches, squeezing increases the binding strength and reduces  $N_c$ . The MFLHY density functional results in larger values for  $N_c$  with respect to the QMC functional, in the range from 13% to 26%. The

functional form used for fitting describes well the energies for numbers of particles close to  $N_c$ , but the particular value of  $N_c$  depends only slightly on the chosen range of clusters included in the fit procedure. The reported error bars for  $N_c$  in Table I include the spread of  $N_c$  values obtained by statistically compatible fits corresponding to different ranges of cluster sizes.

The results for critical numbers of particles obtained with the QMC functional are presented in Table I and compared with obtained MFLHY results for selected cases. For completeness, the results from Ref. [22] for  $f = 1$  are added as well. To facilitate interpretation, we note that lower values of the magnetic field correspond to larger values of  $|\delta a|$ , with  $\delta a = a_{12} + \sqrt{a_{11}a_{22}}$ . For instance, droplets in a  $B = 56.230$  G magnetic field, with  $\delta a = -3.45 \text{ \AA}$  are self-bound with atom numbers smaller than in  $B = 56.639$  G, with  $\delta a = -1.29 \text{ \AA}$ . As a general rule, the binding energy increases with  $|\delta a|$  and so with decreasing  $B$ .

In Fig. 2, we show the dependence of the critical atom number on the oscillator length, for the range of magnetic fields included in Table I. As one can see,  $N_c$  increases with  $a_{ho}$  following an approximately linear behavior. Indeed, the linear function fits well the results for magnetic fields in the range  $B = 56.230$ – $56.453$  G, while for larger values of  $B$  better results are obtained with the functional form  $N_c = N_0 + ca_{ho}^d$ , with  $d$  departing from 1 as the magnetic field is increased. In all cases,  $N_c$  for the lowest studied  $a_{ho}$  are  $\sim 70\%$  lower than the values for  $f = 1$  (the largest  $a_{ho}$  in Fig. 2), which were reported in Ref. [22]. We note that in the range of squeezing studied  $a_{11} \ll a_{ho}$ , which is a prerequisite for using a 3D approximation. Two studies of the crossover from three to two dimensions in a system with periodic boundary conditions determined an additional bound for the validity of the local-density approximation [28,29]. Particularly, in the case of harmonic confinement it was found that the 3D functional can be used when  $\kappa = n_{2D}a_s a_{ho} \gtrsim 1$ , where  $n_{2D}$  is the density integrated over the squeezing direction and  $a_s$  is the scattering length [28]. Using the value of the central density of the large clusters, which corresponds to the saturation density

TABLE I. Critical number of atoms needed to form a bound droplet for different magnetic fields and confinement strengths, described by the harmonic oscillator length  $a_{ho} = f \times 0.639 \mu\text{m}$ . The data in the first row of each section are obtained using the QMC functional, while the data in the second row of each section are obtained by the MFLHY functional. The data for  $f = 1$  are from Ref. [22]. The data in the third row for  $f = 1$  are experimental data from Ref. [2].

$f$	$B(\text{G})$						
	56.230	56.337	56.395	56.453	56.511	56.547	56.639
1	3500	4200	5000	6000	7000	8500	11300
	4650	5570	6200	7000	8050	9800	12700
0.9	3100(50)	3420(855)	3421(855)	4373(1093)	7052(1763)	9217(2304)	13819(3455)
		3800(50)	4650(100)	5400(100)	6250(50)	7400(50)	10300(100)
0.75	2600(50)	4300(100)				8400(100)	
		3200(50)	3900(50)	4550(50)	5200(100)	6100(50)	8350(100)
0.5	1750(50)	3600(50)					
		2200(50)	2550(50)	3000(50)	3400(50)	4200(50)	5700(100)
0.25	970(30)	2600(50)					
		1200(30)	1450(30)	1700(30)	2050(50)	2550(50)	3850(50)
		1400(50)					

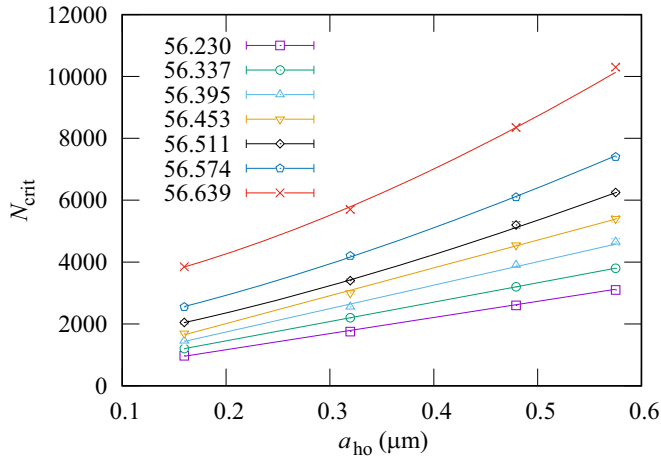


FIG. 2. Critical atom number  $N_c$  needed to form a bound droplet as a function of the harmonic oscillator wavelength  $a_{ho}$ , for different magnetic fields (in G). The error bars are in most cases smaller than the symbol size. The results from Ref. [22], corresponding to the largest  $a_{ho}$ , are marked with larger symbols. The lines represent least-squares fits to data.

of the bulk, and taking the largest scattering length  $a_{11}$ , we have estimated the  $\kappa$  parameter and obtained that, in most cases,  $\kappa \gtrsim 1$ . The exceptions are the strongest confinements for the smaller  $|\delta a|$  (larger magnetic fields), where  $\kappa$  is 0.2, 0.3, 0.4, and 0.6 for  $f = 0.25$ , going from  $B = 56.639$  G to  $B = 56.453$  G, and  $\kappa = 0.6$  for  $f = 0.5$  and  $B = 56.639$  G, while for other parameters it ranges from 1 to almost 22. It was found that the correction to the local-density approximation for systems approaching 2D lowers the ground-state energy [28]. Therefore, it is possible that the density functional for

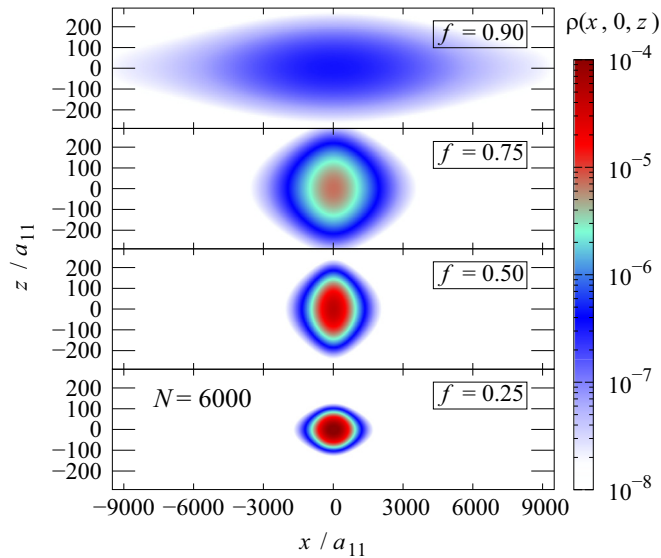


FIG. 3. 2D density profiles  $\rho(x, 0, z)$  of drops with 6000 atoms for the magnetic field  $B = 56.453$  G and different squeezing strengths, described by the harmonic oscillator length of  $a_{ho} = f \times 0.639 \mu\text{m}$ . The profiles are obtained using the QMC functional. Notice the different scales in the direction of the squeezing (vertical) and perpendicular to it.

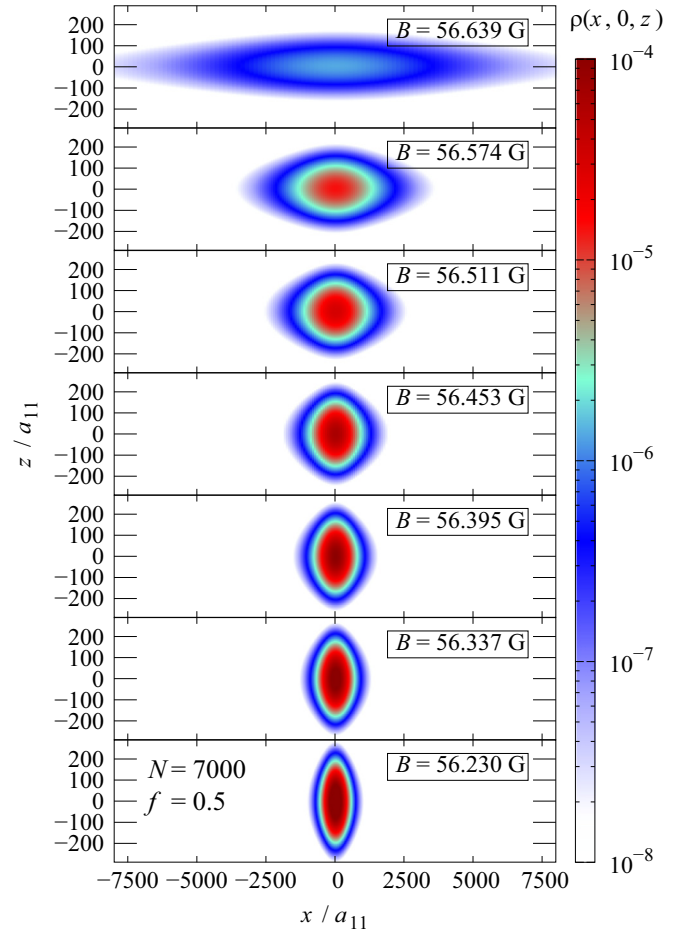


FIG. 4. 2D density profiles  $\rho(x, 0, z)$  of drops with 7000 atoms for different magnetic fields with a fixed squeezing of  $f = 0.5$ . Results are obtained using the QMC functional. Notice the different scales in the direction of the squeezing (vertical) and perpendicular to it.

$\kappa \gtrsim 1$  is missing a confinement-induced correction, which could explain the departure from the linear behavior observed in Fig. 2. Also, as expected using a 3D functional, the lines do not extrapolate to the correct 2D limit,  $N_0 = 2$ , in which clusters of all sizes are bound, as reported in Ref. [27].

The density profiles of the drops are relevant quantities to know their shape and size. By changing the interactions and the squeezing, one can study the effects of confinement and interactions on the size of the clusters. Figure 3 shows the density plots  $\rho(x, 0, z)$  of a drop with 6000 atoms for several squeezing strengths. As the squeezing increases, the half-width of the density profile in the direction of the squeezing,  $\Delta_{\parallel}$ , goes from  $257a_{11}$  for  $f = 0.9$  to  $71a_{11}$  for  $f = 0.25$ . Therefore, even for the tightest confinement the density profile width is significantly larger than the scattering lengths. We observe that the drops are much more extended in the direction perpendicular to squeezing. The chosen drop with  $N = 6000$  particles, in the case of  $f = 0.9$ , is close to the threshold of binding [estimated  $N_c = 5400(100)$ ] and spreads to several thousands of  $a_{11}$  in the direction perpendicular to the confinement (half-width  $\Delta_{\perp} = 6600a_{11}$ , while the width at 10% of the central density is  $15\,000a_{11}$ ). For the strongest squeezing,

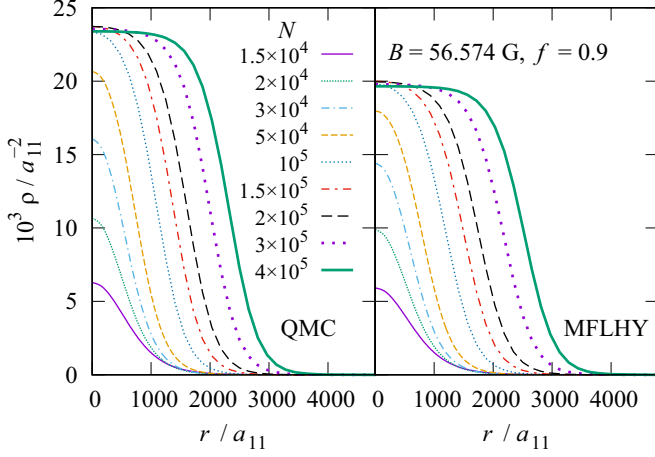


FIG. 5. The density profiles of the drops in the direction perpendicular to squeezing,  $r = \sqrt{x^2 + y^2}$ , obtained with the QMC (left panel) and MFLHY functional (right panel). The squeezing strength is  $f = 0.9$ .

the perpendicular size is reduced by an order of magnitude ( $\Delta_{\perp} = 680a_{11}$ , while the width at 10% of the central density is  $1370a_{11}$ ). The squeezing for the studied range of parameters thus makes the small weakly bound drops less flat, changing the aspect ratio  $\Delta_{\perp}/\Delta_{\parallel}$  from 25.7 for the weakest binding to 9.6 for the strongest one.

It is interesting to explore magnetic field effects on the cluster size for a particular number of particles. Figure 4 shows the density profiles of drops  $\rho(x, 0, z)$  with 7000 atoms for different strengths of the magnetic field and a fixed squeezing of  $f = 0.5$ . With the decrease of the magnetic field, the resulting attractive interaction ( $|\delta a|$ ) increases and thus the drops become more strongly bound and less flattened. Namely, as the attraction is increased, the spread of  $\rho(x, 0, 0)$  distributions is significantly decreased, while the width of  $\rho(0, 0, z)$  distributions is even slightly increased. In the case of the weakest binding ( $B = 56.639$  G), the half-width of the density profile in the direction of squeezing is  $\Delta_{\parallel} = 132a_{11}$ , while the perpendicular one is  $\Delta_{\perp} = 5000a_{11}$ , resulting in  $\Delta_{\perp}/\Delta_{\parallel} \approx 38$ . For the strongest binding ( $B = 56.230$  G) the central density increases 166 times and the size is reduced so that  $\Delta_{\parallel} = 150a_{11}$ ,  $\Delta_{\perp} = 400a_{11}$ , and  $\Delta_{\perp}/\Delta_{\parallel} \approx 2.7$ .

Finally, we present the evolution of the density profiles with the number of particles  $N$  in Figs. 5 and 6. We integrate over  $z$  (the direction of the squeezing) and plot the slice in the perpendicular plane which corresponds to the distribution  $\rho(r)$ , with  $r = \sqrt{x^2 + y^2}$ . The profiles are normalized in such a way that  $2\pi \int \rho(r)rdr = N$ . In both figures, as the number of particles is increased we observe the saturation of the central density, a characteristic property of liquid drops. It is worth noticing the large number of particles in the drop to reach saturation, a consequence of the small binding energy of these so dilute drops. For  $B = 56.574$  G, shown in Fig. 5, the saturation density predicted by the MFLHY functional is about 15% smaller than the QMC one. On the other hand, and similarly to the case of the helium droplets [32,33], for some intermediate size the central density is slightly larger than the saturation density of the equilibrium bulk, a consequence of the surface tension of drops.

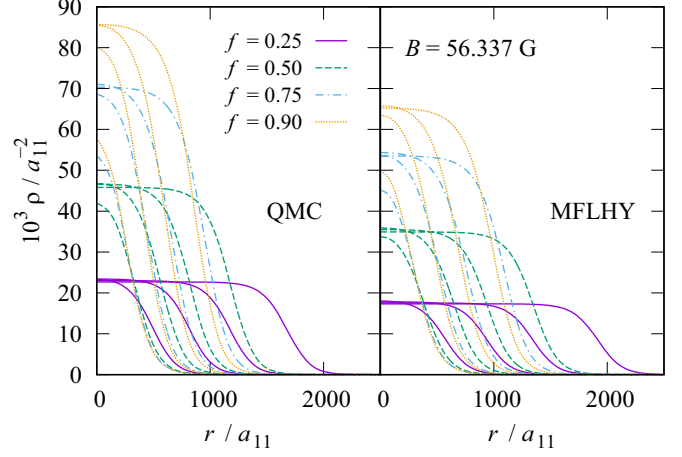


FIG. 6. The density profiles of the drops in the direction perpendicular to squeezing,  $r = \sqrt{x^2 + y^2}$ , calculated by the QMC (left panel) and MFLHY (right panel) functional, for  $B = 56.337$  G. For all  $f$  squeezing intensities, four droplet sizes are shown going from left to right,  $2 \times 10^4$ ,  $5 \times 10^4$ ,  $10^5$ , and  $2 \times 10^5$ .

The saturation density increases with the interparticle attractive interaction strength, but qualitatively the density profiles evolve in the same way with the increase of the droplet size, as shown in Fig. 6 for the case of  $B = 56.337$  G. The plots show four droplet sizes for particle numbers  $2 \times 10^4$ ,  $5 \times 10^4$ ,  $10^5$ , and  $2 \times 10^5$  (from left to right) and for four different confinement strengths. With the increase of the squeezing, the saturation density decreases and it is reached for smaller numbers of particles. Unlike the case of droplets with small numbers of particles shown in Figs. 3 and 4, as the squeezing is increased, the spread of droplets shown in Fig. 6, in the direction perpendicular to squeezing, increases. The difference between the QMC and MFLHY functional predictions grows as the interaction strength is increased, reaching around 24% difference in central density, accompanied with the corresponding change in the spread of the cluster.

#### IV. SUMMARY AND CONCLUSIONS

We have studied the effects of increased confinement on the binding properties, size, and shape of weakly bound Bose-Bose droplets, using a QMC-based density functional. By squeezing the droplets beyond the strength used in the experiment [2], we have observed the decrease of the critical atom number needed to form a droplet, reaching less than 1000 particles for the case of the strongest interparticle interaction ( $B = 56.230$  G) and tightest studied confinement,  $a_{ho} = 0.25 \times 0.639 \mu\text{m}$ . Our results show that, in the observed range of squeezing, the lowering of the critical atom number is approximately linear with the harmonic oscillator length. Deviations from the linear behavior appear for the larger magnetic fields (smaller  $|\delta a|$ ) and the strongest squeezing, signaling the approach of the 3D-2D crossover, where the local-density approximation used may require corrections. It would be useful to perform the full Quantum Monte Carlo calculation in these cases and assess the validity of the functional.

Clusters with the number of particles of the order of  $N_c$  become less flat when the squeezing is increased, which can appear counterintuitive. It can be understood as a consequence of confinement-induced increase of interaction strength. A similar effect appears in very weakly bound helium dimers where significant enhancement of binding and decrease in size are predicted in the planar geometry when the width of the holding potential is approximately equal to the range of the potential [34]. We have also shown that the droplets with small numbers of particles significantly change their aspect ratio when the magnetic field is decreased ( $|\delta a|$  increased), becoming significantly less flat for the weakest magnetic field (most strongly bound droplet) considered.

As the number of particles in the cluster is increased, the central density increases and reaches saturation. After clusters reach the central density's saturation, the increase in confinement strength makes them extend perpendicularly to the direction of squeezing, in a manner which is very similar to the behavior of helium clusters [33]. Bose-Bose saturated drops are observed only when the number of atoms are orders of magnitude larger than  $N_c$ , hindering their experimental observation due to three-body losses.

Finally, our work points to the possibility of controlling droplet size and binding by adjusting the harmonic confinement in one direction. Increase of measurement precision would also enable discerning the effects beyond the LHY term, which are most prominent for  $B = 56.230$  G, corresponding to the most strongly bound droplets, when they amount to around 25% of the energy and central density.

#### ACKNOWLEDGMENTS

We acknowledge financial support from Ministerio de Ciencia e Innovación MCIN/AEI/10.13039/501100011033 (Spain) under Grant No. PID2020-113565GB-C21 and from AGAUR-Generalitat de Catalunya under Grant No. 2021-SGR-01411. The computational resources of the server UniST-Phy at the University of Split were used.

TABLE II. Scattering lengths  $a_{ij}$  for the  $^{39}\text{K}$  mixture (in units of Bohr's radius  $a_0$ ) and the parameters  $\alpha$ ,  $\beta$ , and  $\gamma$  of the equation of state, as a function of magnetic field  $B$  (in G).  $\alpha$  is given in units of  $\hbar^2 a_{11}/2m$ ,  $\beta$  is given in units of  $\hbar^2 a_{11}^{3\gamma-2}/2m$ , and  $\gamma$  is dimensionless.

$B(\text{G})$	$a_{11}(a_0)$	$a_{22}(a_0)$	$a_{12}(a_0)$	$\alpha(\frac{\hbar^2 a_{11}}{2m})$	$\beta(\frac{\hbar^2 a_{11}^{3\gamma-2}}{2m})$	$\gamma$
56.230	63.648	34.587	-53.435	-0.812	5.974	1.276
56.337	66.619	34.369	-53.386	-0.640	6.281	1.301
56.395	68.307	34.252	-53.360	-0.513	7.701	1.347
56.453	70.119	34.136	-53.333	-0.423	8.549	1.373
56.511	71.972	34.020	-53.307	-0.358	8.851	1.379
56.574	74.118	33.895	-53.278	-0.294	8.359	1.382
56.639	76.448	33.767	-53.247	-0.203	12.152	1.440

#### APPENDIX

The values of the scattering lengths and effective ranges for selected magnetic field strengths are given in Table II, together with the values of the density functional parameters reported in Ref. [35].

In order to solve the Schrödinger equation in imaginary time, we propagate the wave function  $\psi$  with the time-evolution operator

$$\psi(\tau + \Delta\tau) = e^{-\Delta\tau H} \psi(\tau). \quad (\text{A1})$$

To this end, we have implemented a three-dimensional numerical solver based on the Trotter decomposition of the time-evolution operator [36] with second-order accuracy in the time step  $\Delta\tau$  as follows:

$$e^{-\Delta\tau H} \approx e^{-\Delta\tau V(\mathbf{R}')/2} e^{-\Delta\tau K} e^{-\Delta\tau V(\mathbf{R})/2} + O((\Delta\tau)^2), \quad (\text{A2})$$

with  $K$  and  $V$  being the kinetic and potential terms in Eq. (2).

To solve the equations, particles were put in a box, adjusting its size to be wider than the system. It was verified that the size of the box and the discretization of the space do not bias the results.

- [1] D. S. Petrov, Quantum mechanical stabilization of a collapsing Bose-Bose mixture, *Phys. Rev. Lett.* **115**, 155302 (2015).
- [2] C. Cabrera, L. Tanzi, J. Sanz, B. Naylor, P. Thomas, P. Cheiney, and L. Tarruell, Quantum liquid droplets in a mixture of Bose-Einstein condensates, *Science* **359**, 301 (2018).
- [3] G. Semeghini, G. Ferioli, L. Masi, C. Mazzinghi, L. Wolswijk, F. Minardi, M. Modugno, G. Modugno, M. Inguscio, and M. Fattori, Self-bound quantum droplets of atomic mixtures in free space, *Phys. Rev. Lett.* **120**, 235301 (2018).
- [4] I. Ferrier-Barbut, H. Kadau, M. Schmitt, M. Wenzel, and T. Pfau, Observation of quantum droplets in a strongly dipolar Bose gas, *Phys. Rev. Lett.* **116**, 215301 (2016).
- [5] M. Schmitt, M. Wenzel, F. Böttcher, I. Ferrier-Barbut, and T. Pfau, Self-bound droplets of a dilute magnetic quantum liquid, *Nature (London)* **539**, 259 (2016).
- [6] H. Kadau, M. Schmitt, M. Wenzel, C. Wink, T. Maier, I. Ferrier-Barbut, and T. Pfau, Observing the Rosensweig instability of a quantum ferrofluid, *Nature (London)* **530**, 194 (2016).
- [7] C. D'Errico, A. Burchianti, M. Prevedelli, L. Salasnich, F. Ancilotto, M. Modugno, F. Minardi, and C. Fort, Observation of quantum droplets in a heteronuclear bosonic mixture, *Phys. Rev. Res.* **1**, 033155 (2019).
- [8] Z. Guo, F. Jia, L. Li, Y. Ma, J. M. Hutson, X. Cui, and D. Wang, Lee-Huang-Yang effects in the ultracold mixture of  $^{23}\text{Na}$  and  $^{87}\text{Rb}$  with attractive interspecies interactions, *Phys. Rev. Res.* **3**, 033247 (2021).
- [9] Z.-H. Luo, W. Pang, B. Liu, Y.-Y. Li, and B. A. Malomed, A new form of liquid matter: Quantum droplets, *Front. Phys.* **16**, 32201 (2021).
- [10] F. Böttcher, J.-N. Schmidt, J. Hertkorn, K. S. H. Ng, S. D. Graham, M. Guo, T. Langen, and T. Pfau, New states of matter with fine-tuned interactions: quantum droplets and dipolar supersolids, *Rep. Prog. Phys.* **84**, 012403 (2021).

- [11] C. J. Pethick and H. Smith, *Bose-Einstein Condensation in Dilute Gases* (Cambridge University, Cambridge, England, 2008).
- [12] T. D. Lee, K. Huang, and C. N. Yang, Eigenvalues and eigenfunctions of a Bose system of hard spheres and its low-temperature properties, *Phys. Rev.* **106**, 1135 (1957).
- [13] D. M. Larsen, Binary mixtures of dilute Bose gases with repulsive interactions at low temperature, *Ann. Phys.* **24**, 89 (1963).
- [14] V. Cikojević, K. Dželalija, P. Stipanović, L. Vranješ Markić, and J. Boronat, Ultradilute quantum liquid drops, *Phys. Rev. B* **97**, 140502(R) (2018).
- [15] H. Hu and X.-J. Liu, Consistent theory of self-bound quantum droplets with bosonic pairing, *Phys. Rev. Lett.* **125**, 195302 (2020).
- [16] H. Hu, J. Wang, and X.-J. Liu, Microscopic pairing theory of a binary Bose mixture with interspecies attractions: Bosonic BEC-BCS crossover and ultradilute low-dimensional quantum droplets, *Phys. Rev. A* **102**, 043301 (2020).
- [17] N. Guebli and A. Boudjemâa, Quantum self-bound droplets in Bose-Bose mixtures: Effects of higher-order quantum and thermal fluctuations, *Phys. Rev. A* **104**, 023310 (2021).
- [18] S. Giorgini, J. Boronat, and J. Casulleras, Ground state of a homogeneous Bose gas: A diffusion Monte Carlo calculation, *Phys. Rev. A* **60**, 5129 (1999).
- [19] M. Rossi, L. Salasnich, F. Ancilotto, and F. Toigo, Monte Carlo simulations of the unitary Bose gas, *Phys. Rev. A* **89**, 041602(R) (2014).
- [20] C. Staudinger, F. Mazzanti, and R. E. Zillich, Self-bound Bose mixtures, *Phys. Rev. A* **98**, 023633 (2018).
- [21] V. Cikojević, L. Vranješ Markić, G. E. Astrakharchik, and J. Boronat, Universality in ultradilute liquid Bose-Bose mixtures, *Phys. Rev. A* **99**, 023618 (2019).
- [22] V. Cikojević, L. Vranješ Markić, and J. Boronat, Finite-range effects in ultradilute quantum drops, *New J. Phys.* **22**, 053045 (2020).
- [23] V. Cikojević, L. Vranješ Markić, M. Pi, M. Barranco, and J. Boronat, Towards a quantum Monte Carlo-based density functional including finite-range effects: Excitation modes of a  $^{39}\text{K}$  quantum droplet, *Phys. Rev. A* **102**, 033335 (2020).
- [24] H. Hu and X.-J. Liu, Collective excitations of a spherical ultradilute quantum droplet, *Phys. Rev. A* **102**, 053303 (2020).
- [25] G. Ferioli, G. Semeghini, L. Masi, G. Giusti, G. Modugno, M. Inguscio, A. Gallemí, A. Recati, and M. Fattori, Collisions of self-bound quantum droplets, *Phys. Rev. Lett.* **122**, 090401 (2019).
- [26] V. Cikojević, L. Vranješ Markić, M. Pi, M. Barranco, F. Ancilotto, and J. Boronat, Dynamics of equilibration and collisions in ultradilute quantum droplets, *Phys. Rev. Res.* **3**, 043139 (2021).
- [27] D. S. Petrov and G. E. Astrakharchik, Ultradilute low-dimensional liquids, *Phys. Rev. Lett.* **117**, 100401 (2016).
- [28] T. Ilg, J. Kumlin, L. Santos, D. S. Petrov, and H. P. Büchler, Dimensional crossover for the beyond-mean-field correction in Bose gases, *Phys. Rev. A* **98**, 051604(R) (2018).
- [29] P. Zin, M. Pylak, T. Wasak, M. Gajda, and Z. Idziaszek, Quantum Bose-Bose droplets at a dimensional crossover, *Phys. Rev. A* **98**, 051603(R) (2018).
- [30] P. Zin, M. Pylak, Z. Idziaszek, and M. Gajda, Self-consistent description of Bose-Bose droplets: Modified gapless Hartree-Fock-Bogoliubov method, *New J. Phys.* **24**, 113038 (2022).
- [31] P. Zin, M. Pylak, and M. Gajda, Self-consistent description of Bose-Bose droplets: Harmonically trapped quasi-two-dimensional droplets, *Phys. Rev. A* **106**, 013320 (2022).
- [32] S. Stringari and J. Treiner, Systematics of liquid helium clusters, *J. Chem. Phys.* **87**, 5021 (1987).
- [33] J. Mur-Petit, A. Sarsa, J. Navarro, and A. Polls, Density functional study of two-dimensional  $^4\text{He}$  clusters, *Phys. Rev. B* **72**, 104513 (2005).
- [34] S. Kilić, E. Krotscheck, and L. Vranješ, Binding of two helium atoms in confined geometries. II. Dimerization on flat attractive substrates, *J. Low Temp. Phys.* **119**, 715 (2000).
- [35] V. Cikojević, *Ab-initio* quantum Monte Carlo study of ultracold atomic mixtures (2021), available at <https://urn.nsk.hr/urn:nbn:hr:217:633063>.
- [36] S. A. Chin, S. Janecek, and E. Krotscheck, Any order imaginary time propagation method for solving the Schrödinger equation, *Chem. Phys. Lett.* **470**, 342 (2009).